

The Gas-to-Dust Relation in the Dark Cloud L1523 - Observational Evidence for CO Gas Depletion

H. G. Kim, B. G. Kim and J. H. Jung

Korea Astronomy and Space Science Institute, 61-1, Hwaam, Yuseong, Daejeon 305-348, Korea;
hgkim@kasi.re.kr

Received 2007 November 9; accepted 2008 March 10

Abstract Correlation between gas and dust column density has been studied for the dark globule L1523. The $^{13}\text{CO}(J=1\rightarrow 0)$ emission is used for tracing the gas, and the IR emissions, for tracing the dust constituent. In order to match the beam resolution between the images, a beam de-convolution algorithm based on the Maximum Correlation Method (MCM) was applied on the Infrared Astronomical Satellite (IRAS) data. The morphology of ^{13}CO column density map shows a close correlation to that of $100\ \mu\text{m}$ dust optical depth. The distribution of the optical depth at $100\ \mu\text{m}$ follows that of gas column density more closely than does the flux map at either 60 or $100\ \mu\text{m}$. The ratio of the ^{13}CO column density to the $100\ \mu\text{m}$ optical depth shows a decreasing trend with increasing dust optical depth in the central part, indicating possible molecular gas condensation onto dust particles. The excessive decrease in the CO column density in the envelope may most probably be due to the photo-dissociation of CO molecules.

Key words: ISM: clouds — ISM: dust — ISM: molecules

1 INTRODUCTION

Dark clouds are composed almost entirely of molecular hydrogen. Since the molecular hydrogen cannot be observed directly, tracers other than molecular hydrogen are often used when probing dark clouds. Therefore, we more often investigate the rotational transition lines of diatomic molecules such as CO molecules which, though less abundant than the molecular hydrogen, are more easily detected.

However, we must be careful when using the CO molecule as a mass tracer, because even within a given cloud the abundance of CO relative to H_2 may vary from the center to the envelope. In sufficiently dense and cold regions of the cloud core, the CO molecules are likely to condense onto dust (Dessauges-Zavadsky et al. 2007), while in the outer regions they will be dissociated by the UV photons of the interstellar radiation field (ISRF). These circumstances affect the CO abundance relative to those of dust and molecular hydrogen. If the possibilities of condensation and dissociation are ignored, and a constant ratio of CO-to- H_2 abundance is assumed, then we shall underestimate the H_2 column density.

Lines of evidence for depletion of gas have been reported. CO molecules in solid state have been observed in several dense cores of the ρ Ophiuchi, Taurus and Serpens molecular clouds (Whittet et al. 1989; Kerr et al. 1993; Chiar et al. 1994; Fraser et al. 2005). These facts indicate that the condensation of molecular species onto dust does occur in such dense clouds. A theoretical study by Bergin et al. (1995) also showed that the CO molecules can be depleted with respect to H_2 by condensing onto dust. The depletion may amount to a factor of 3 in a time scale of 10^7 years, when $n(\text{H}_2) \sim 10^4\ \text{cm}^{-3}$ and the gas kinetic temperature and dust temperature are 20 K and 10 K, respectively. The depletion factor becomes even larger as $n(\text{H}_2)$ increases. When the $n(\text{H}_2)$ is $10^5\ \text{cm}^{-3}$, almost complete depletion of CO from gas phase occurs in a period of 10^7 years. These observational and theoretical studies strongly suggest that the condensation of CO molecules onto dust does occur, at least in the central part of dark globules.

On the other hand, the CO molecules located in the outer regions of a dark cloud, where dust is not dense enough to shield the interstellar UV radiation, are easily dissociated. Glassgold et al. (1985) investigated how the abundance of CO isotopes is affected by the photo-dissociation process under the interstellar UV radiation field. Their results showed that a significant change in the CO-to-H₂ abundance may occur, depending on the local physical conditions over the cloud boundary extending A_V up to 2 magnitudes.

Therefore, it is interesting to check how much variation one may see in the ratio of the CO column density to the dust optical depth in the visual or IR, as one moves from the globule center to the periphery. The extinction obtained from star counts analysis can be a good measure of the CO column densities in the outer regions of dark clouds. However, in the opaque dense cores, the same star count method provides us with poor measures of extinction. This is because the extinction determined by star counts is only a lower limit to the true extinction in regions where no stars are seen through. On the other hand, the dark clouds are extremely thin at IR wavelengths. At the IR wavelengths one can look deep into the cores, which are completely opaque in the optical wavelength, and the CO emission is even saturated there. Thus, the optical depth in the IR rather than the visible acts as a good mass tracer in the dense regions of the dark clouds.

The Infrared Astronomical Satellite (IRAS) has provided us with an excellent data base. With four IR bands centered at 12, 25, 60 and 100 μm , the satellite surveyed about 95% of the whole sky. The FWHM responses are $0.75' \times 4.45'$, $0.75' \times 4.65'$, $1.50' \times 4.76'$ and $3.00' \times 5.05'$ at the four bands, respectively. The spatial resolution of the IRAS beams does not totally suffice for our purpose, so we decide to de-convolute the IRAS images with the beam pattern and to use the de-convoluted images for our comparative study.

In this paper, we will compare the column density of CO and the IR optical depth in a dark globule named L1523. Among the 12 dark globules of Kim & Hong (2002), L1523 was selected because it is well isolated and shows the narrowest $^{13}\text{CO}(J=1 \rightarrow 0)$ line width, indicating cold, quiet internal physical condition and therefore possible CO depletion. From this study, we will answer the following two questions: (1) Can we confirm that CO depletion occurs in the cores of small dark globules observationally? (2) Can we confirm that photo-dissociation of CO molecules operates in the outer regions of the dark globules?

In Section 2 we show the CO integrated intensity distribution. We carry out an analysis of IRAS data in Section 3. In Section 4 we will examine correlation between the gas column density and the IR dust optical depth. Section 5 presents the conclusions.

2 CO INTEGRATED INTENSITY DISTRIBUTION

All the CO data are taken from Kim & Hong (2002). A brief description for the observations is as follows. The 4 m Radio Telescope of the Nagoya University was used to collect both $^{12}\text{CO}(J=1 \rightarrow 0)$ and $^{13}\text{CO}(J=1 \rightarrow 0)$ spectra during the observing season 1996 – 1997. The HPBW of the Nagoya 4 m antenna is about $2.7'$ at the rest frequency of the $^{13}\text{CO}(J=1 \rightarrow 0)$ transition. Spectra were taken in frequency switching mode with a spatial sampling rate of $2'$. In total, 221 (13×17) points were observed in the $^{13}\text{CO}(J=1 \rightarrow 0)$ transition, and only cross scans across the peak position of $^{13}\text{CO}(J=1 \rightarrow 0)$ emission were made in $^{12}\text{CO}(J=1 \rightarrow 0)$ transition. A cooled SIS mixer receiver was used for the frontend. The receiver temperature at the $^{13}\text{CO}(J=1 \rightarrow 0)$ transition was typically 150 K. All the data were collected with the 1024 channel acousto-optical spectrometer at a frequency resolution of 48 kHz, which corresponds to a velocity resolution of 0.13 km s^{-1} at 110 GHz. The frequency switching was done at intervals of 13 MHz, or 35 km s^{-1} at 110 GHz. The system temperatures were typically about 400 K and 300 K at the ^{12}CO and ^{13}CO transitions, respectively. After a 5 minute integration the rms noise temperature of the ^{13}CO spectra was typically about 0.2 K. The resulting signal to noise ratios were greater than 10 for the globule center. The pointing accuracy and antenna gain were checked regularly by observing a standard source. The antenna temperature T_A^* of the standard source varied by less than 5% during the entire period of observations.

The resulting maps of the $^{13}\text{CO}(J=1 \rightarrow 0)$ integrated intensity are overlaid on the Palomar Observatory Sky Survey (POSS) red print, see Figure 1. The area enclosed with dashed lines denotes the region observed in the ^{13}CO emission. The $^{13}\text{CO}(v_i)$ column density in each velocity channel v_i was calculated on the LTE assumptions of Dickman (1978) and Penzias (1975). The results of the LTE analysis toward the peak position of L1523 are summarized in Table 1. The distance to L1523 was taken from Wu et al. (1992).

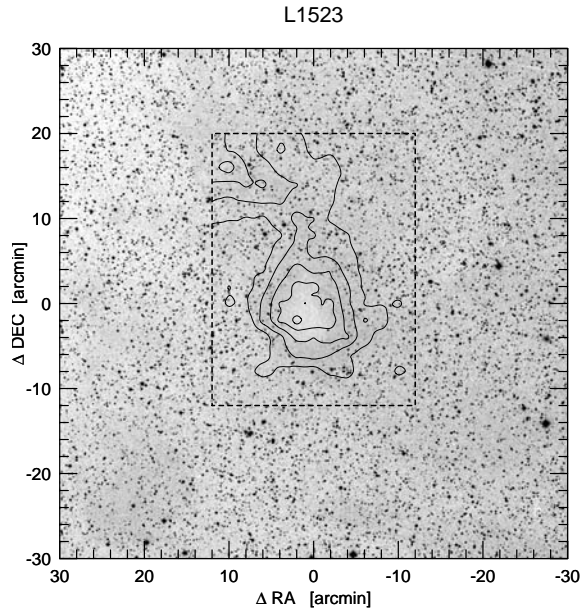


Fig. 1 Contours of the integrated radiation temperature of the $^{13}\text{CO}(J=1\rightarrow 0)$ emission overlaid on the POSS red print. The area enclosed with dashed lines denotes the region observed in the ^{13}CO emission. The $(0, 0)$ position is $(\alpha_{\text{B1950}}, \delta_{\text{B1950}}) = (5^{\text{h}}03^{\text{m}}00^{\text{s}}, 31^{\circ}40'00'')$, and the contour levels increase from 0.5 K km s^{-1} with a step of 0.5 K km s^{-1} .

Table 1 Results of the LTE Analysis toward the Peak Position of L1523

Globule	T_{ex} (K)	$^{13}\tau_0$	$N(^{13}\text{CO})$ (10^{15} cm^{-2})	Radius (pc)	Turbulence (km s^{-1})	Total Mass (M_{\odot})	Distance (pc)
L1523	12	0.7	3.7	0.23	0.75	17	140

3 ANALYSIS OF THE IRAS DATA

The IRAS focal plane was originally designed to detect infrared point sources (IRAS Catalogs and Atlases, 1988, Vols. 1–6), and the shape of the detector and the scan strategy were not optimized for studying extended sources. Moreover, the spatial resolution of the $60 \mu\text{m}$ image is different from that of the $100 \mu\text{m}$ image, and even more different from that of CO observations. However, the IR fluxes at these two wavelength bands provide crucial information for the cold dust component of the dark globules (Hong et al. 1991). In order to use the IRAS data for a comparative study of the internal structure of an isolated cloud, one must apply beam de-convolution.

Another problem in using the IRAS data is the extremely small optical depths at the IRAS wavelengths (order of 10^{-4} at $100 \mu\text{m}$). This means that the IRAS sky flux toward a globule has contributions from both the background radiation and the globule itself. In order to obtain the flux emitted by the dark globule itself, one must correct for the flux emanating from the background.

3.1 Image Deconvolution

As described in Section 1, the spatial resolutions of the IRAS co-added images are highly elongated and the beam sizes are about $1.50' \times 4.76'$ at $60 \mu\text{m}$, and $3.00' \times 5.05'$ at $100 \mu\text{m}$. Moreover, the beam shapes are different from image to image due to the combined effect of different detector response functions and different scanning directions of the satellite, and also due to the coarse and the non-uniform sampling.

On the other hand, the HPBW of Nagoya 4 m Radio Telescope is $2.7'$. In order to make a meaningful comparison of the data, matching of the spatial resolution of the IRAS data is required.

The observed image can be treated as the result of convolution of the true image and the point spread function (PSF). In order to determine the PSF for L1523, we inspected all the point-like sources in the 60 and $100\ \mu\text{m}$ images. A best candidate for the PSF should preferably be symmetric and free from contamination by the diffuse emission, and must be found at the same position in both images at 60 and $100\ \mu\text{m}$. We determine the PSF by fitting the image profile with two dimensional elongated Gaussian surface.

Various methods have been developed for the beam de-convolution or the restoration of an astronomical blurry image (Richardson 1972; Lucy 1974; Frieden & Aumann 1987; Jefferies & Christou 1993). All the algorithms discussed in the literature require to know the PSF and the manner of blurring of the images. None of these algorithms works for the resolution enhancement of the IRAS images, because the IRAS images are not blurred images, rather, they are images obtained from irregular and over-sampled data (nicknamed footprints) taken by detectors of different spatial resolutions. For the purpose of the IRAS image de-convolution, we adopted the Maximum Correlation Method (MCM) developed by Aumann et al. (1990). Actually the MCM does not restore the blurred image, but re-constructs the original image from the irregular, over-sampled data, and thereby enhances the resolution. The MCM relies basically on the Richardson-Lucy algorithm (Richardson 1972; Lucy 1974). The main difference between the MCM and the original Richardson-Lucy algorithm is that the Richardson-Lucy algorithm requires the input data on rectangular grids and a single PSF, while the MCM does not need the grid to be regular nor the PSF to be unique. The MCM collects the non-uniformly distributed data and from them it iteratively constructs the original image. In this respect, the MCM does *not* de-convolute an image, but re-creates an image and restores resolution. If the input data are on rectangular grid points with the same noise and the PSF is symmetric and the same at every data points, then the two methods become identical.

However, the MCM algorithm in Aumann et al. (1990) was aimed at the aperture photometry of strong IRAS point sources, and is not suitable for the de-convolution of an extended object like a dark globule, which tended to enhance strong point-like sources in the image and depresses the diffuse emission from dark clouds. So we compiled our own version of MCM with adjustable convergence parameter suitable for the de-convolution of a dark globule. In our version we improved the Aumann et al. (1990)'s algorithm by taking advantage of the flexibility of the Interactive Data Language (IDL). We applied the revised algorithm to the $100\ \mu\text{m}$ full resolution survey coadd (FRESCO) image of L1523. The resulting de-convoluted FRESCO image at $100\ \mu\text{m}$ has a spatial resolution comparable to those of the $60\ \mu\text{m}$ image.

3.2 Background Removal

Due to the extremely thin optical depth in the IR wavelengths, the IRAS image is contaminated by various kinds of background emission. Although the FRESCO image is already corrected for the emission from the zodiacal cloud, it still contains contributions from background sources other than the globule itself. For our comparative study of gas and dust, the background components should be removed.

For the background removal, one must determine the boundary for a given cloud. Considering that any emission from outside of the boundary could be regarded as background, we inspected both the radio and visual extinction maps and determined their background levels by selecting a set of control pixels located at some distances outside of the CO boundary. Once the control pixels were selected, the same set of control pixels was used for both $60\ \mu\text{m}$ and $100\ \mu\text{m}$ images. We then fit the image values at the control pixels with a smooth spline surface. This surface was regarded as the background image, and subtracted from the original image. Since the resulting boundary after the removal depends on the selection of the control pixels, the background removal process repeated a few times. In most cases, 20 control pixels with three iterations were enough to fit the background surface.

3.3 Dust Optical Depth

The following simplifying conditions are assumed for the IRAS images of the dark globules: the physical parameters including the dust temperature do not vary much along the line of sight. The wavelength dependency of the dust absorption efficiency factor $Q_{\text{abs}}(\lambda)$ follows a power-law of the form, $Q_{\text{abs}}(\lambda) \propto \lambda^{-n}$.

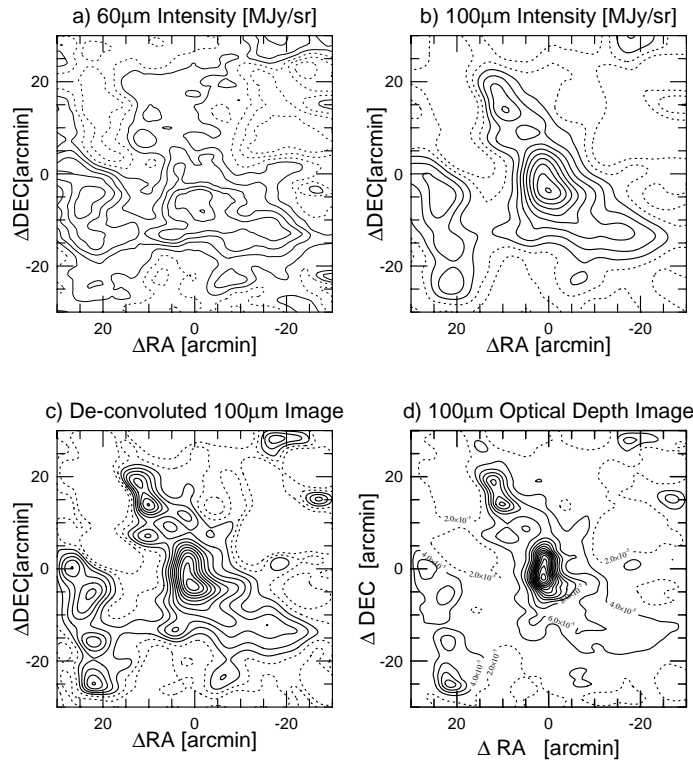


Fig. 2 Original FRESKO images at $60\ \mu\text{m}$ (a) and at $100\ \mu\text{m}$ (b). The de-convoluted $100\ \mu\text{m}$ image is shown in (c), and (d), the final dust optical depth τ_λ contour map at $100\ \mu\text{m}$. The contour levels start at optical depth 2×10^{-5} and increase at steps of 2×10^{-5} .

Then the grain temperature can be obtained from the flux densities at two wavelengths according to

$$T_d \simeq \frac{hc}{k} \left[\frac{1}{\lambda_{60}} - \frac{1}{\lambda_{100}} \right] / \ln \left[\frac{I_{100}}{I_{60}} \left(\frac{\lambda_{100}}{\lambda_{60}} \right)^{3+n} \right], \quad (1)$$

I_λ being the intensity at wavelength λ . The value n is not precisely known and is thought to be in the range $1 \leq n \leq 2$. According to Draine & Lee (1984), if the dust particles are composed of pure silicate, then $n \simeq 2$; while if graphite, then n will be somewhat smaller. In this study we adopt $n = 1.5$ for all the globules. The dust optical depth τ_λ is then obtained from the relation

$$I_\lambda = B_\lambda(T_d) \tau_\lambda, \quad (2)$$

on the assumption that the line of sight is optically thin. $B_\lambda(T_d)$ is the Planck function.

Figure 2a to 2d show the original FRESKO images at 60 and $100\ \mu\text{m}$ supplied by the IPAC, the de-convoluted $100\ \mu\text{m}$ image, and the final dust optical depth τ_λ map calculated from the de-convoluted 60 and $100\ \mu\text{m}$ images. In Figure 2d we can recognize a structure with a scale down to $\sim 2.5'$, and a flux enhancement by a factor of about 2 for the $100\ \mu\text{m}$ image. Since the total flux is conserved during the iterations in our beam de-convolution algorithm, the square root of the peak intensity ratio corresponds directly to the ratio of resolution enhancement of ~ 1.4 .

4 CORRELATION BETWEEN ^{13}CO COLUMN DENSITY AND IR OPTICAL DEPTH

In order to examine the gas-to-dust ratio within the cloud, we plot $N(^{13}\text{CO})$ versus $I(100\ \mu\text{m})$ in Figure 3 and versus $\tau_d(100\ \mu\text{m})$ in Figure 4. In both figures, the upper dotted line represents the linear least squares

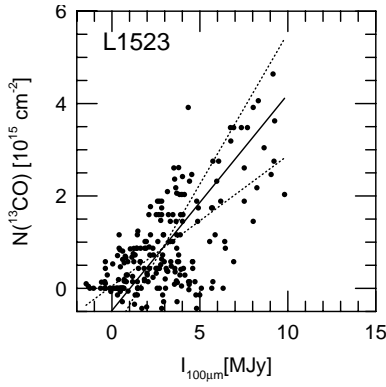


Fig. 3 Scatter plot of $N(^{13}\text{CO})$ as a function of $I(100\ \mu\text{m})$. Solid line represents the result of linear regression. See the text for dotted lines.

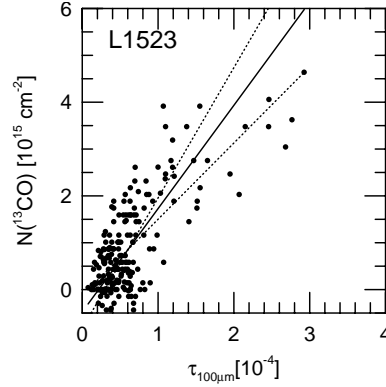


Fig. 4 Scatter plot of $N(^{13}\text{CO})$ as a function of $\tau_d(100\ \mu\text{m})$. Solid line represents the result of linear regression. See the text for dotted lines.

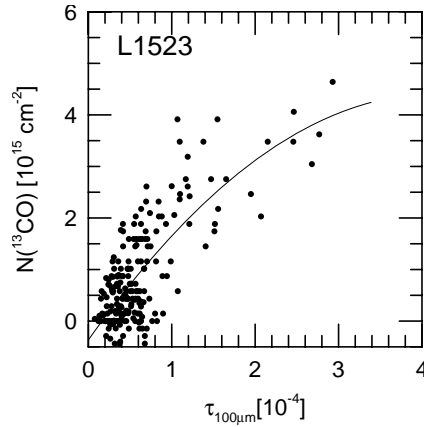


Fig. 5 Scatter plots of $N(^{13}\text{CO})$ as a function of $\tau_d(100\ \mu\text{m})$. Solid line represents the result of the least squares fit with a second order polynomial.

fits that minimized the deviations in the direction of $\tau_d(100\ \mu\text{m})$, while the lower one, in the direction of $N(^{13}\text{CO})$. The solid lines represent the mean relation. Comparing Figure 3 with Figure 4, we see that the $N(^{13}\text{CO}) - \tau_d(100\ \mu\text{m})$ correlation is much tighter than that of $N(^{13}\text{CO}) - I(100\ \mu\text{m})$.

From Figure 4, the mean relation between $N(^{13}\text{CO}) - \tau_d(100\ \mu\text{m})$ was found to be:

$$\left[\frac{N(^{13}\text{CO})}{10^{15}\ \text{cm}^{-2}} \right] = (2.2 \pm 0.6) \left[\frac{\tau_d(100\ \mu\text{m})}{10^{-4}} \right] - (0.4 \pm 0.3). \quad (3)$$

This slope is much less steep than those for $\rho\ \text{Oph}$ (~ 4.1) (Jarrett et al. 1989) or B5 (~ 6.3) (Langer et al. 1989), indicating possible depletion of CO molecules in the dense part of the globule.

If the gas-to-dust ratio is uniform within the globule, the scatter plot would show a linear relation. However, we carefully examined Figure 4 and found that the observed points can be better fitted by a polynomial rather than by a straight line. This forced us to use a second order polynomial in the least squares fitting. As seen in Figure 5, the $N(^{13}\text{CO}) - \tau_d(100\ \mu\text{m})$ relation can be fitted better by a second order polynomial than by a straight line. The least squares fit curves are convex upward: as one goes deep into the globule, $N(^{13}\text{CO})$ increases less rapidly than $\tau_d(100\ \mu\text{m})$ does. This may indicate that (1) the CO molecules are condensed onto the dust in the dense part of the globule, and (2) the CO molecules locating near the globule boundary are dissociated by the UV photons from the ISRF.

There are three possible explanations to the rapid decrease of $N(^{13}\text{CO})$ in the envelope (wang et al. 2004). They are (1) thin optical depth of ^{12}CO , or (2), selective photo-dissociation of ^{13}CO molecules by UV radiation field, or (3), abnormal abundance variation of ^{13}CO relative to ^{12}CO . If the ^{12}CO is optically thin, the less abundant molecule of ^{13}CO can not be detected at all. However, in L1523 the optical depth of ^{13}CO is 0.7 at the center and about 0.1 at the boundary, and that of ^{12}CO is already well saturated even in the envelope. Therefore, the optically thin case can be ruled out for L1523. The possibility of abnormal abundance variation along the radial distance seems not to be feasible in such a small dark cloud with a radius of 0.23 pc and with a turbulence velocity of 0.75 km s^{-1} . Hence, the photo-dissociation process may be the most plausible explanation. Since the optically thick ^{12}CO molecules can shield themselves from the UV photons, then the optically thinner ^{13}CO molecules can be easily destroyed selectively. This process can result in the decrease of ^{13}CO intensity in the envelope even though the $^{12}\text{C}/^{13}\text{C}$ ratio remains unchanged.

5 CONCLUSIONS

From the correlation study above, we draw the following conclusions: (1) For L1523, the $N(^{13}\text{CO})$ vs. $\tau_d(100 \mu\text{m})$ relation shows a less steep slope than those for other clouds, and the relation is better fitted by a polynomial of order 2 rather than by a linear function. (2) The decreasing trend of the CO column density relative to the dust optical depth toward the cloud center may indicate that molecular gas condenses onto dust particles in the dense part of dark globules. (3) The excessive decrease in the CO column density in the envelope is most possibly due to the photo-dissociation by the UV photons from ISRF.

References

- Aumann H. H., Fowler J. W., Melnyk M., 1990, *AJ*, 99, 1674
 Bergin E. A., Langer W. D., Goldsmith P. F., 1995, *ApJ*, 441, 222
 Chiar J. E., Adamson A. J., Kerr T. H., Whittet D. C. B., 1994, *ApJ*, 426, 240
 Dessauges-Zavadsky M., Combes F., Pfenniger D., 2007, *A&A*, 473, 863
 Dickman R. L., 1978, *ApJS*, 37, 407
 Draine B. T., Lee H. M., 1984, *ApJ*, 285, 89
 Fraser H. J., Bisschop S. E., Pontoppidan K. M. et al., 2005 *MNRAS*, 356, 1283
 Frieden R. B., Aumann H. H. G., 1987, *Appl. Opt.*, 26, 3615
 Glassgold A. E., Huggins P. J., Langer W. D., 1985, *ApJ*, 290, 615
 Hong S. S., Kim H. G., Park S. H., Park Y. S., Imaoka K., 1991, *J. Kor. Ast. Soc.*, 24, 71
 Jarrett T. H., Dickman R. L., Herbst W., 1989, *ApJ*, 345, 881
 Jefferies S. M., Christou J. C., 1993, *ApJ*, 415, 862
 Kerr T. H., Adamson A. J., Whittet D. C. B., 1993, *MNRAS*, 262, 1047
 Kim H. G., Hong S. S., 2002, *ApJ*, 567, 376
 Langer W. D., Wilson R. W., Goldsmith P. F., Beichman C. A., 1989, *ApJ*, 337, 355
 Lucy L. B., 1974, *AJ*, 79, 745
 Penzias A. A., 1975, in: *Atomic and Molecular Physics and Interstellar Matter*, eds. R. Balian, P. Encrenaz, J. Lequeux, New York: American Elsevier
 Richardson W. H., 1972, *J. Opt. Soc. Am.*, 62, 55
 Wang J., Chen W., Miller M., Qin S., Wu Y., 2004, *ApJ*, 614, L105
 Whittet D. C. B., Adamson A. J., Duley W. W., Geballe T. R., McFadzean A. D., 1989, *MNRAS*, 241, 707
 Wu Y., Zhou S., Evans II N. J., 1992, *ApJ*, 394, 196